Self-assembly of Taper-shaped Monoesters of Oligo(ethylene oxide) with 3,4,5-Tris(*p*-dodecyloxybenzyloxy)benzoic Acid and of their Polymethacrylates into Tubular Supramolecular Architectures Displaying a Columnar Mesophase

Virgil Percec,*[a] James Heck,[a] Dimitris Tomazos,[a] Frederick Falkenberg,[a] Helen Blackwell[a] and Goran Ungar*[b]

[a] *Department of Macromolecular Science, Case Western Reserve University, Cleveland, OH 44106-2699, USA*

[b] *Department of Engineering Materials and Centre for Molecular Materials, The University of Sheffield, Sheffield, S1 3DU, UK*

The taper-shaped monoesters of mono- **3a**, di- **3c**, tri- **3d**, and tetra- **3f** ethylene glycol with 3,4,5-*tris*(*p*-dodecyloxybenzyloxy)benzoic acid **1** and their corresponding polymethacrylates, **6a**, **b**, **c** and **d**, respectively, self-assemble into a tubular supramolecular architecture displaying an enantiotropic columnar hexagonal (Φ_h) mesophase. Characterization of this supramolecular architecture by a combination of differential scanning calorimetry, wide- and small-angle X-ray scattering, thermal optical polarized microscopy, and molecular modelling suggests a model in which the stratum of the column is formed by in between 3.9 and 5.4 molecules of **3** or 4.5 and 5.9 repeat units of **6** with their oligo(oxyethylenic) segments melted and segregated in the centre of the column and their melted alkyl tails radiating towards the columns periphery. 2-(2-Methoxyethyl) 3,4,5-tris(*p*-dodecyloxybenzyloxy)benzoate **3b** (the model compound of **3a** in which the hydroxy group has been replaced by a methoxy group) is only crystalline, while bis(2-{2-[3,4,5-tris(*p*-dodecyloxybenzyloxy)benzoyloxy]ethoxy}ethyl) ether **3g** (which is the dimer of **3c**) displays a monotropic Φ_h phase. These results support that *endo*-recognition by H-bonding of the oligo(oxyethylenic)receptor of **3** and *exo*-recognition provided by the tapered 3,4,5-tris(*p*-dodecyloxybenzyloxy)benzoate fragment of **3** (most probably functioning by hydrophobic–hydrophobic interactions) provide the driving force for the self-assembly of this tubular supramolecular architecture. In the case of the supramolecular architectures derived from **6**, the H-bonding interaction is replaced by the poly(methacrylate) backbone which leads to a Φ_h mesophase that undergoes isotropization at temperatures that are 40 °C higher than those of **3**. The channel penetrating the middle of the supramolecular cylinders derived from both **3** and **6** dissolves alkali-metal triflates and the ionic interaction generated by the dissolved ion-pairs enhances the thermal stability of their Φ_h phase. These results allowed for the first time a comparison between a 'molecular' polymer backbone effect (polymethacrylate) and a 'supramolecular' polymer backbone effect (generated by way of H-bonding and ionic interactions) to be made.

Presently we are investigating various synthetic approaches to the self-assembly[1] of tubular supramolecular architectures by employing principles which resemble those used by Tobacco Mosaic Virus (TMV).[1d-f] TMV was selected as a model since it represents the best understood self-assembled biological system. In the first series of experiments reported,[2] we used as a driving force for the self-assembly process a combination of *exo*-recognition generated by a tapered structural unit and a living polymerization reaction. The polymerization reaction replaces the *endo*-recognition process and helps in the selection of the most suitable tapered structural unit which can be used further in the self-assembling process which functions only by a combination of *endo*- and *exo*-recognition.[3] The 3,4,5-tris(*p*-alkyloxybenzyloxy)benzoate group was selected as the basic component of the tapered structural unit which is used in our present investigations.[2,3] 4'-Methyl(benzo-15-crown-5)-3,4,5-tris(4-dodecyloxybenzyloxy)benzoate forms a layered crystal structure.[3] The complexation of its benzo-15-crown-5 *endo*-receptor with $NaCF_3SO_3$ or KCF_3SO_3 destabilizes its crystalline phase and induces its self-assembly into a cylindrical architecture which displays an enantiotropic thermotropic columnar hexagonal (Φ_h) mesophase. The stratum of the self-assembled column is formed by about 5.8 tapered structural units which have their benzo-15-crown-5 receptors placed side by side in the centre of the column and their melted alkyl tails radiating towards its periphery. *endo*-Recognition generated *via* the benzo-15-crown-5 receptor upon complexation and *exo*-recognition due to the tapered 3,4,5-tris(*p*-dodecyloxybenzyloxy)benzoate fragment of the structural unit provide the driving force for the self-assembly of this cylindrical supramolecular architecture.[3]

The goal of this paper is to report a novel, more efficient and conceptually simpler structural unit which is derived from 4'-methyl(benzo-15-crown-5)-3,4,5-tris(4-dodecyloxybenzyloxy)-benzoate by replacing its selective benzo-15-crown-5 *endo*-receptor with the non-selective hydroxyoligo(oxyethylene) group containing from one to four oxyethylenic (OE) units. The hydroxyoligo(oxyethylenic) *endo*-receptor functions by a combination of hydrogen bonding and nonselective complexation of metal salts. The corresponding poly(methyl methacrylates) will be discussed and will allow for the first time a comparison between a 'molecular' and a 'supramolecular' polymer backbone effect to be made.

Experimental

Tetraethylene glycol (99%), triethylene glycol (99%), tetrabutylammonium hydrogen sulfate (TBAH, 97%), toluenesulfonyl chloride (98%), 2-methoxyethanol (99%) (all from Aldrich), 4-dimethylaminopyridine (DMAP, 98%, Fluka), methacryloyl chloride (97%, Fluka), ethylene glycol (Fisher), diethylene glycol (Pfaltz & Bauer), trifluoromethanesulfonic

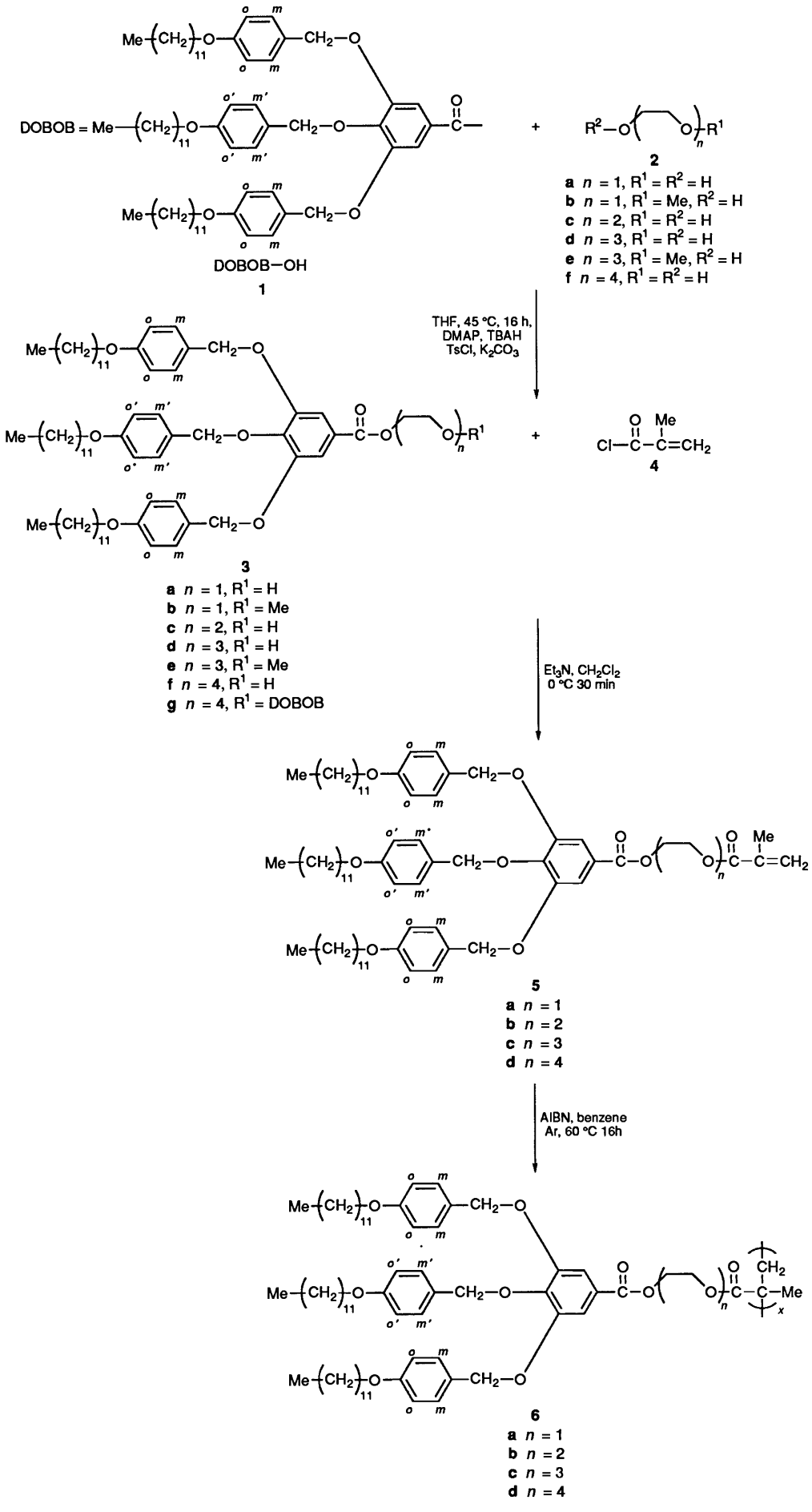

Scheme 1 Synthesis of ω-hydroxyoligo(oxyethylene) 3,4,5-tris(*p*-dodecyloxybenzyloxy)benzoates and ω-methoxyoligo(oxyethylene)3,4,5-tris(*p*-dodecyloxybenzyloxy)benzoates **3**, and of the polymers based on ω-methacryloyloxyoligo(oxyethylene) 3,4,5-tris(*p*-dodecyloxybenzyloxy)benzoates **6**

acid (triflic acid, 98%, Johnson Matthew Catalog Co.), and the other conventional reagents were used as received. Triethylene glycol monomethyl ether (95%, Aldrich) was distilled *in vacuo* (141 °C/0.35 mmHg) and the first and last 10% of material that distilled was discarded. Tetrahydrofuran (THF) was distilled from $LiAlH_4$. Triethylamine (Et_3N) was heated overnight at 60 °C over KOH, distilled from KOH, and then stored over KOH. Benzene was washed with 50 cm^3 portions of H_2SO_4 until they remained relatively uncoloured, washed with water to neutral pH, dried over $MgSO_4$, filtered, heated at 80 °C overnight over $LiAlH_4$, and then was distilled. $LiCF_3SO_3$ (97%, Aldrich) was dried at 120 °C *in vacuo* for 24 h. $NaCF_3SO_3$ was synthesized by adding triflic acid to a solution of NaOH in MeOH cooled to 0 °C until a pH of 1 was obtained (determined by pH paper). Excess of MeOH was evaporated on a rotary evaporator and the resultant solid was stirred in CH_2Cl_2 at reflux for 10 min and then was filtered off. The last step with CH_2Cl_2 was repeated twice. The resultant solid was dried for 48 h at 120 °C, m.p. 249–250 °C (lit.,[4] m.p. 248 °C). 2,2'-Azoisobutyronitrile (AIBN, Fluka) was recrystallized from MeOH below 40 °C.

Techniques.—^1H NMR (200 MHz) spectra were recorded on a Varian XL-200 spectrometer. Infrared (IR) spectra were recorded on a Perkin-Elmer 1320 infrared spectrometer. Relative molecular weights of polymers were measured by gel permeation chromatography (GPC) with a Perkin-Elmer Series 10 LC instrument equipped with an LC-100 column oven and a Nelson 900 series integrator data station. A set of two Polymer Laboratories PL gel columns of 5 × 10^2 and 10^4 Å and $CHCl_3$ as solvent (1 cm^3 min^{-1}) was used. The measurements were made at 40 °C using a UV detector. Polystyrene standards were used for the calibration plot. High-pressure liquid chromatography (HPLC) experiments were performed with the same instrument. A Perkin-Elmer DSC-4 differential scanning calorimeter equipped with a TADS data station was used to determine the thermal transitions which were reported as the maximum and minimum of their endothermic and exothermic peaks. In all cases, heating and cooling rates were 20 °C min^{-1} unless specified. Glass transition temperatures (T_g) were read at the middle of the change in heat capacity. First heating scans differ from second and subsequent heating scans. However, second and subsequent heating scans are identical. The difference between various DSC scans will be discussed. X-Ray scattering patterns were recorded using either a helium-filled flat-plate wide angle (WAXS) camera or a pinhole-collimated small angle (SAXS) camera. Ni-filtered Cu-Kα radiation was used. The samples were in the form of: (a) as prepared polymers in the form of powder or (b) bulk samples in Lindemann thin-walled 1-mm capillaries cooled from the melt. The temperature stability of the X-ray heating cell was ±0.1 °C. A Carl-Zeiss optical polarized microscope (magnification × 100x) equipped with a Mettler FP82 hot stage and a Mettler FP80 central processor was used to observe the thermal transitions and to analyse the anisotropic textures. Molecular modelling was done using CSC Chem3D™ from Cambridge Scientific Computing, Inc.

Scheme 1 outlines the synthesis of all compounds which will be discussed in this paper.

3,4,5-*Tris*(*p-dodecyloxybenzyloxy*)*benzoic Acid* **1**.—The synthesis of **1** has been described earlier;[5,6] purity: 99% (HPLC); thermal transitions are reported in Table 1; $\delta_H(CDCl_3$, TMS) 0.88 (t, 9 H, CH_3), 1.27 [overlapped peaks, 54 H, $(CH_2)_9$], 1.79 (overlapped peaks, 6 H, $CH_2CH_2OC_6H_4$), 3.97 (overlapped peaks, 6 H, $CH_2CH_2OC_6H_4$), 5.03 (s, 2 H, OC_6H_4–CH_2-OC_6H_2–CO_2 from 4-position), 5.06 (s, 4 H, $OC_6H_4CH_2$-OC_6H_2–CO_2 from 3- and 5-positions), 6.76 (d, 2 H, $OC_6H_4CH_2OC_6H_2CO_2$ *o'*-H, *J* 8.9), 6.90 (d, 4 H, OC_6H_4-$CH_2OC_6H_2CO_2$ *o*-H, *J* 8.4), 7.26 (d, 2 H, $OC_6H_4CH_2CO_2$ *m'*-H, *J* 8.3), 7.34 (d, 4 H, $OC_6H_4CH_2OC_6H_2CO_2$ *m*-H, *J* 8.7) and 7.43 (s, 2 H, $C_6H_2CO_2H$); ν_{max}(KBr plate)/cm^{-1} 1690 (C=O).

Compounds **3a–g** were synthesized using a similar procedure. A representative example is presented for **3a**.

2-*Hydroxyethyl* 3,4,5-*Tris*(p-*dodecyloxybenzyloxy*)*benzoate* **3a**.—The acid **1** (6.00 g, 6.04 mmol) ethylene glycol (2.62 g, 4.22 mmol), TsCl (1.09 g, 5.72 mmol), DMAP (0.20 g, 1.64 mmol), TBAH (0.20 g, 0.59 mmol), anhydrous K_2CO_3 (2.50 g, 18.1 mmol) and dry THF (30 cm^3) were mixed in a flask and then sealed with a stopper and heated and stirred at 45 °C for 16 h. The reaction mixture was allowed to cool and the precipitate was filtered off. The filtrate was slowly poured into water (1 cm^3) that had been slightly acidified with HCl and the mixture cooled to 0 °C. The resultant precipitate was then filtered off, dissolved in THF and then precipitated again by addition of the solution to ice–water; this procedure was repeated twice. The solid was allowed to dry in air and then purified by flash chromatography (neutral alumina, THF eluent) to remove inorganic salts. After solvent evaporation, the product was purified by column chromatography (silica gel, $CHCl_3$ eluent) to yield **3a** as a white solid (4.24 g, 68%); purity 99% (HPLC); thermal transitions are reported in Table 1; $\delta_H(CDCl_3$, TMS) 0.86 (t, 9 H, CH_3), 1.26 [overlapped peaks, 54 H, $(CH_2)_9$], 1.72 (overlapped peaks, 6 H, $CH_2CH_2OC_6H_4$), 3.92 (overlapped peaks, 8 H, $CH_2CH_2OC_6H_4$ and CH_2OH), 4.38 (t, 2 H, CH_2O_2C, *J* 4.5), 5.00 (s, 2 H, $OC_6H_4CH_2OC_6H_2$-CO_2 from 4-position), 5.03 (s, 4 H, $OC_6H_4CH_2OC_6H_2CO_2$ from 3- and 5-positions), 6.74 (d, 2 H, $OC_6H_4CH_2OC_6H_2CO_2$ *o'*-H, *J* 7.1), 6.87 (d, 4 H, $OC_6H_4CH_2OC_6H_2CO_2$ *o*-H, *J* 9.1), 7.22 (d, 2 H, $OC_6H_4CH_2OC_6H_2CO_2$, *m'*-H, *J* 7.7), 7.31 (d, 4 H, $C_6H_4CH_2OC_6H_2CO_2$, *m*-H, *J* 9.7), 7.35 (s, 2 H, $C_6H_2CO_2$); ν_{max}(KBr)/cm^{-1} 3410 (*v*-OH) and 1700 (C=O).

2-*Methoxyethyl* 3,4,5-*Tris*(p-*dodecyloxybenzyloxy*)*benzoate* **3b**.—The acid **1** (1.00 g, 1.01 mmol), ethylene glycol monomethyl ether **2b** (0.30, 3.94 mmol), TsCl (0.23 g, 1.21 mmol), DMAP (0.05 g, 0.41 mmol), TBAH (0.05, 0.15 mmol) and K_2CO_3 (2.00 g, 14.5 mmol) gave **3b** as a white solid (0.33 g, 31%); purity 99% (HPLC). Thermal transitions are reported in Table 1. $\delta_H(CDCl_3$, TMS) 0.88 (t, 9 H, $CH_3)_3$, 1.26 [overlapped peaks, 54 H, $(CH_2)_9$], 1.76 (overlapped peaks, 6 H, $CH_2CH_2OC_6H_4$), 3.42 (s, 3 H, OCH_3), 3.71 (t, 2 H, CH_3OCH_2, *J* 4.3), 3.94 (overlapped peaks, 6 H, $CH_2CH_2OC_6H_4$), 4.43 (t, 2 H, CH_2O_2C, *J* 4.6), 5.00 (s, 2 H, $OC_6H_4CH_2OC_6H_2CO_2$ from 4-position), 5.04 (s, 4 H, $OC_6H_4CH_2OC_6H_2CO_2$ from 3- and 5-positions), 6.74 (d, 2 H, $OC_6H_4CH_2OC_6H_2CO_2$ *o'*-H, *J* 8.2), 6.89 (d, 4 H, $OC_6H_4CH_2OC_6H_2CO_2$ *o*-H, *J* 8.4), 7.24 (d, 2 H, $OC_6H_4CH_2OC_6H_2CO_2$ *m'*-H, *J* 8.5), 7.33 (d, 4 H, OC_6H_4-$CH_2OC_6H_2CO_2$ *m*-H, *J* 8.6) and 7.37 (s, 2 H, $C_6H_2CO_2$); ν_{max}(KBr)/cm^{-1} 1715 (C=O).

2-(2-*Hydroxyethoxy*)*ethyl* 3,4,5-*Tris*(p-*dodecyloxybenzyloxy*)*benzoate* **3c**.—The acid **1** (5.00 g, 5.03 mmol), diethylene glycol **2c** (5.30 g, 49.4 mmol), TsCl (0.93 g, 4.88 mmol), DMAP (0.10 g, 0.89 mmol), TBAH (0.10 g, 0.29 mmol) and K_2CO_3 (5.00 g, 36.2 mmol) gave **3c** as a white solid (2.64 g, 48%); purity: 99% (HPLC). Thermal transitions are reported in Table 1; $\delta_H(CDCl_3$, TMS), 0.86 (t, 9 H, CH_3), 1.21 [overlapped peaks, 54 H, $(CH_2)_9$], 1.73 (overlapped peaks, 6 H, $CH_2CH_2OC_6H_4$), 3.65 (t, 2 H, CH_2OH, *J* 3.9), 3.75 (t, 2 H, CH_2CH_2OH, *J* 3.3), 3.82 (t, 2 H, $CH_2CH_2O_2C$, *J* 4.4), 3.94 (overlapped peaks, 6 H, $CH_2CH_2OC_6H_4$), 4.46 (t, 2 H, CH_2O_2C, *J* 4.2), 5.00 (s, 2 H, $OC_6H_4CH_2OC_6H_2CO_2$ from 4-position), 5.04 (s, 4 H, $OC_6H_4CH_2OC_6H_2CO_2$ from 3- and 5-positions), 6.74 (d, 2 H,

$OC_6H_4CH_2OC_6H_2CO_2$ *o'*-H, *J* 8.1), 6.88 (d, 4 H, OC_6H_4-$CH_2OC_6H_2CO_2$ *o*-H, *J* 7.7), 7.24 (d, 2 H, $OC_6H_4CH_2OC_6H_2$-CO_2 *m'*-H, *J* 8.4), 7.32 (d, 4 H, $OC_6H_4CH_2OC_6H_2CO_2$ *m*-H, *J* 8.6), 7.36 (s, 2 H, Ph*H*–CO_2); ν_{max}(Kbr plate)/cm^{-1} 3410 (OH) and 1705 (C=O).

2-[2-(2-*Hydroxyethoxy*)*ethoxy*]*ethyl* 3,4,5-*Tris*(p-*dodecyloxybenzyloxy*)*benzoate* **3d**.—The acid **1** (5.10 g, 5.10 mmol), triethylene glycol **2d** (3.07 g, 20.0 mmol), TsCl (0.95 g, 5.00 mmol), DMAP (0.20 g, 1.60 mmol), TBAH (0.20 g, 0.80 mmol) and K_2CO_3 (3.00, 22.0 mmol) gave **3d** as a white solid (3.90 g, 69%); purity: 99% (HPLC). Thermal transitions are reported in Table 1; δ_H($CDCl_3$, TMS) 0.89 (t, 9 H, CH_3), 1.28 [overlapped peaks, 54 H, $(CH_2)_9$], 1.78 (overlapped peaks, 6 H, $CH_2CH_2OC_6H_4$), 2.41 (br, 1 H, OH), 3.60 (t, 2 H, CH_2OH, *J* 5.1), 3.70 (s, 6 H, OCH_2CH_2O), 3.83 (t, 2 H, $CH_2CH_2O_2C$, *J* 4.5), 3.95 (overlapped peaks, 6 H, $CH_2CH_2OC_6H_4$), 4.47 (t, 2 H, CH_2OOC, *J* 4.7), 5.00 (s, 2 H, $OC_6H_4CH_2OC_6H_2CO_2$ from 4-position), 5.05 (s, 4 H, $OC_6H_4CH_2OC_6H_2CO_2$ from 3- and 5-positions), 6.75 (d, 2 H, $OC_6H_4CH_2OC_6H_2CO_2$, *o'*-H, *J* 9.6), 6.89 (d, 4 H, $OC_6H_4CH_2OC_6H_2CO_2$, *o*-H, *J* 9.6), 7.24 (d, 2 H, $OC_6H_4CH_2OC_6H_2CO_2$, *m'*-H, *J* 9.1), 7.33 (d, 4 H, $OC_6H_4CH_2OC_6H_2CO_2$, *m*-H, *J* 8.4) and 7.40 (s, 2 H, $C_6H_2CO_2$), ν_{max}(KBr plate)/cm^{-1} (OH) and 1710 (C=O).

2-{2-[2-(2-*Methoxy*)*ethoxy*]*ethoxy*}*ethyl* 3,4,5-*Tris*(p-*dodecyloxybenzyloxy*)*benzoate* **3e**.—The acid **1** (3.00 g, 3.02 mmol), triethylene glycol monomethyl ether **2e** (1.50 g, 9.73 mmol), TsCl (0.57 g, 2.99 mmol), DMAP (0.20 g, 1.68 mmol), TBAH (0.02, 0.59 mmol), and K_2CO_3 (2.00 g, 14.5 mmol) gave **3e** as a white solid (0.67 g, 19%); purity 99% (HPLC); m.p. 52 °C (DSC at 20 °C min^{-1}); δ_H($CDCl_3$, TMS) 0.85 (t, 9 H, CH_3), 1.23 [overlapped peaks, 54 H, $(CH_2)_9$], 1.73 (overlapped peaks, 6 H, $CH_2CH_2OC_6H_4$), 3.32 (s, 3 H, CH_3OCH_2), 3.48 (t, 2 H, CH_2OCH_3, *J* 3.9), 3.64 (overlapped peaks, 6 H, OCH_2CH_2O), 3.74 (t, 2 H, $CH_2CH_2O_2C$, *J* 4.5), 3.90 (overlapped peaks, 6 H, $CH_2CH_2OC_6H_4$), 4.40 (t, 2 H, CH_2O_2C, *J* 4.1), 5.00 (s, 2 H, $OC_6H_4CH_2CO_2$ from 4-position), 5.04 (s, 4 H, $OC_6H_4CH_2$-$OC_6H_2CO_2$ 3- and 5-positions), 6.75 (d, 2 H, $OC_6H_4CH_2OC_6$-H_2CO_2, *o'*-H, *J* 8.9), 6.89 (d, 4 H, $OC_6H_4CH_2OC_6H_2CO_2$, *o*-H, *J* 8.2), 7.24 (d, 2 H, $OC_6H_4CH_2OC_6H_2CO_2$, *m'*-H, *J* 8.7), 7.33 (d, 4 H, $OC_6H_4CH_2OC_6H_2CO_2$, *m*-H, *J* 8.7) and 7.37 (s, 2 H, $C_6H_2CO_2$); ν_{max}(KBr plate)/cm^{-1} 1700 (C=O).

2-{2-[2-(2-*Hydroxyethoxy*)*ethoxy*]*ethoxy*}*ethyl* 3,4,5-*Tris*(p-*dodecyloxybenzyloxy*)*benzoate* **3f**.—The acid **1** (5.10 g, 5.10 mmol), tetraethylene glycol **2f** (9.91 g, 51.0 mmol), TsCl (0.97 g, 5.10 mmol), DMAP (0.20 g, 1.68 mmol), TBAH (0.20 g, 0.59 mmol) and K_2CO_3 (3.00 g, 21.7 mmol) gave **3f** as a white solid (3.73 g, 63%); purity: 99% (HPLC); thermal transitions are reported in Table 1; δ_H($CDCl_3$, TMS) 0.88 (t, 9 H, CH_3), 1.30 [overlapped peaks, 54 H, $(CH_2)_9$], 1.70 (overlapped peaks, 6 H, $CH_2CH_2OC_6H_4$), 3.50 (t, 2 H, CH_2OH, *J* 3.7), 3.64, 3.68 (2 overlapped singlets, 10 H, OCH_2CH_2O), 3.82 (t, 2 H, $CH_2CH_2O_2C$, *J* 4.1), 3.94 (overlapped peaks, 6 H, $CH_2CH_2OC_6H_4$), 4.40 (t, 2 H, CH_2O_2C, *J* 5.2), 4.99 (s, 2 H, $OC_6H_4CH_2OC_6H_2CO_2$ from 4-position), 5.08 (s, 4 H, $OC_6H_4CH_2OC_6H_2CO_2$ from 3- and 5-positions), 6.74 (d, 2 H, $OC_6H_4CH_2OC_6H_2CO_2$ *o'*-H, *J* 8.7), 6.88 (d, 4 H, OC_6H_4-$CH_2OC_6H_2CO_2$ *o*-H, *J* 7.9), 7.23 (d, 2 H, $OC_6H_4CH_2OC_6H_2$-CO_2, *m'*-H, *J* 8.4), 7.32 (d, 4 H, $OC_6H_4CH_2OC_6H_2CO_2$, *m*-H, *J* 8.1) and 7.36 (s, 2 H, $C_6H_2CO_2$), ν_{max}(KBr plate) 3440 (OH) and 1705 (C=O).

Bis(2-{2-[3,4,5-*tris*(p-*dodecyloxybenzyloxy*)*benzoyloxy*]*ethoxy*}*ethyl*) *Ether* **3g**.—The acid **1** (3.00 g, 3.02 mmol), tetraethylene glycol **2f** (0.26 g, 1.33 mmol), TsCl (0.70 g, 3.67 mmol), DMAP (0.05 g, 0.41 mmol), TBAH (0.05, 0.15 mmol) and K_2CO_3 (3.00 g, 21.7 mmol) gave **3g** as a white solid (0.41 g, 13%); purity: 99% (HPLC); thermal transitions are reported in Table 1; δ_H($CDCl_3$, TMS) 0.88 (t, 18 H, CH_3), 1.28 [overlapped peaks, 108 H, $(CH_2)_9$], 1.73 (overlapped peaks, 12 H, $CH_2CH_2OC_6H_4$), 3.62 (s, 8 H, OCH_2CH_2O), 3.79 (t, 4 H, $CH_2CH_2O_2C$, *J* 5.3), 3.94 (overlapped peaks, 12 H, $CH_2CH_2OC_6H_4$), 4.42 (t, 4 H, CH_2O_2C, *J* 5.3), 4.98 (s, 4 H, $OC_6H_4CH_2OC_6H_2CO_2$ from 4-position), 5.01 (s, 8 H, $OC_6H_4CH_2OC_6H_2CO_2$ from 3- and 5-positions), 6.73 (d, 4 H, $OC_6H_4CH_2OC_6H_2CO_2$, *o'*-H, *J* 8.3), 6.87 (d, 8 H, $OC_6H_4CH_2OC_6H_2CO_2$, *o*-H, *J* 8.7), 7.22 (d, 4 H, OC_6H_4-$CH_2OC_6H_2CO_2$, *m'*-H, *J* 8.5), 7.33 (d, 8 H, $OC_6H_4CH_2$-$OC_6H_2CO_2$ *m*-H, *J* 9.0), 7.34 (s, 4 H, $C_6H_2CO_2$); ν_{max}(KBr plate)/cm^{-1} 1715 (C=O).

Compounds **5a–d** were synthesized using a similar procedure. An example is given below for compounds **5a**.

2-*Methacryloyloxyethyl* 3,4,5-*Tris*(p-*dodecyloxybenzyloxy*)-*benzoate* **5a**.—Compound **3a** (2.00, 1.9 mmol), methacryoloyl chloride **4** (0.74 g, 7.7 mmol) and dry CH_2Cl_2 (25 cm^3) were mixed in a 100 cm^3 round-bottom flask equipped with anhydrous $CaCl_2$ drying tube and the reaction mixture was cooled to 0–5 °C in an ice–water bath. Dry Et_3N (1.40 cm^3, 10.0 mmol) was added dropwise to the reaction mixture which was then stirred at 0–5 °C for 1 h. After this it was poured in water and extracted with CH_2Cl_2 (100 cm^3). The extract was washed several times with 5% aqueous HCl and water and then dried ($MgSO_4$) and evaporated on a rotary evaporator at room temperature. The crude product was then dissolved in THF (20 cm^3) and the solution poured into cold methanol–water (1:1, v/v; 200 cm^3) to precipitate the product which was filtered off and dried *in vacuo*. Further purification by column chromatography (neutral alumina, THF) yielded the monomer **5a** (1.21 g, 57%); purity: 99% (HPLC); m.p. 58–59 °C; δ_H($CDCl_3$, TMS) 0.88 (t, 9 H, CH_3), 1.26 [overlapped peaks, 54 H, $(CH_2)_9$], 1.75 (overlapped peaks, 6 H, $CH_2CH_2OC_6H_4$), 1.95 (s, 3 H, $CH_3C{=}CH_2$), 3.95 (overlapped peaks, 6 H, $CH_2OC_6H_4$), 4.50 (overlapped peaks, 4 H, $CO_2CH_2CH_2$), 5.00 (s 2 H, $OC_6H_4CH_2OC_6H_2CO_2$ from 4-position), 5.03 (s, 4 H, $OC_6H_4CH_2OC_6H_2CO_2$ from 3- and 5-positions), 5.59 [s, 1 H, $C(CH_3){=}CH_2$ *trans* to C=O], 6.14 [s, 1 H, $C(CH_3){=}CH_2$ *cis* to C=O], 6.75 (d, 2 H, $OC_6H_4CH_2OC_6H_2CO_2$, *o'*-H, *J* 9.2), 6.88 (d, 4 H, $OC_6H_4CH_2OC_6H_2CO_2$, *o*-H, *J* 8.3), 7.24 (d, 2 H, $-OC_6H_4CH_2OC_6H_2CO_2$, *m'*-H, *J* 8.8), 7.32 (d, 4 H, $OC_6H_4CH_2OC_6H_2CO_2$, *m*-H, *J* 8.8) and 7.35 (s, 2 H, $C_6H_2CO_2$); ν_{max}(KBr plate)/cm^{-1} 1715 (C=O).

2-(2-*Methacryloyloxyethoxy*)*ethyl* 3,4,5-*Tris*(p-*dodecyloxybenzyloxy*)*benzoate 5b*.—Compound **3c** (2.00 g, 1.9 mmol), **4** (0.71 cm^3, 7.4 mmol) and Et_3N (1.34 cm^3, 9.6 mmol) gave **5b** (1.12 b, 53%); purity 99% (HPLC); m.p. 53–54 °C; δ_H($CDCl_3$, TMS) 0.88 (t, 9 H, CH_3), 1.27 [overlapped peaks, 54 H, $(CH_2)_9$], 1.75 (overlapped peaks, 6 H, $CH_2CH_2OC_6H_4$), 1.90 (s, 3 H, $CH_3C{=}CH_2$), 3.80 (overlapped peaks, 4 H, $CH_2CH_2O_2C$), 3.95 (overlapped peaks, 6 H, $CH_2OC_6H_4$), 4.32 [t, 2 H, $CH_2O_2CC(CH_3)$, *J* 4.5], 4.44 (t, 2 H, CH_2CO_2, *J* 5.1), 5.00 (s, 2 H, $OC_6H_4CH_2OC_6H_2CO_2$ from 4-position), 5.03 (s, 4 H, $OC_6H_4CH_2OC_6H_2CO_2$ from 3- and 5-positions), 5.51 [s, 1 H, $C(CH_3){=}CH_2$ *trans* to C=O], 6.09 [s, 1 H, $C(CH_3){=}CH_2$ *cis* to C=O], 6.74 (d, 2 H, $OC_6H_4CH_2OC_6H_2CO_2$, *o'*-H, *J* 8.1), 6.89 (d, 4 H, $OC_6H_4CH_2OC_6H_2CO_2$, *o*-H, 8.3), 7.23 (d, 2 H, $OC_6H_4CH_2OC_6H_2CO_2$, *m'*-H, *J* 8.0), 7.32 (d, 4 H, $OC_6H_4CH_2$-$OC_6H_2CO_2$ *m*-H, *J* 8.7) and 7.36 (s, 2 H, $C_6H_2CO_2$); ν_{max}(KBr plate)/cm^{-1} 1715 (C=O).

2-[2-(2-*Methacryloyloxyethoxy*)*ethoxy*]*ethyl* 3,4,5-*Tris*(p-*dodecyloxybenzyloxy*)*benzoate* **5c**.—Compound **3d** (2.90 g, 2.6 mmol), **4** (1.00 cm^3, 10.4 mmol), and Et_3N (2 cm^3, 14.6 mmol),

gave **5c** (2.46 g, 80%); purity: 99% (HPLC); m.p. 59–60 °C; δ_H($CDCl_3$, TMS) 0.88 (t, 9 H, CH_3), 1.26 (overlapped peaks, 54 H, $(CH_2)_9$], 1.75 (overlapped peaks, 6 H, $CH_2CH_2OC_6H_4$), 1.93 [s, 3 H, $CH_3C{=}CH_2$), 3.68 (s, 6 H, OCH_2CH_2O), 3.81 (t, 2 H, $CCO_2CH_2CH_2$, J 5.0), 3.95 (overlapped peaks, 6 H, $CH_2OC_6H_4$), 4.29 [t, 2 H, CH_2O_2C–$C(CH_3)$, *J* 5.1], 4.44 (t, 2 H, CO_2CH_2, *J* 4.4), 5.00 (s, 2 H, $OC_6H_4CH_2OC_6H_2CO_2$ from 4-position), 5.03 (s, 4 H, $OC_6H_4CH_2OC_6H_2CO_2$ from 3-and 5-positions), 5.54 [s, 1 H, $C(CH_3){=}CH_2$ *trans* to C=O], 6.11 [s, 1 H, $C(CH_3){=}CH_3){=}CH_2$ *cis* to C=O], 6.74 (d, 2 H, $OC_6H_4CH_2OC_6H_2CO_2$– *o'*-H, *J* 8.2), 6.88 (d, 4 H, $OC_6H_4CH_2OC_6H_2CO_2$– *o*-H *J* 8.2), 7.23 (d, 2 H, $OC_6H_4CH_2OC_6H_2CO_2$– *m'*-H, *J* 7.8), 7.32 (d, 4 H, $OC_6H_4CH_2OC_6H_2CO_2$– *m*-H, *J* 8.2) and 7.37 (s, 2 H, $C_6H_2CO_2$); ν_{max}(KBr plate)/cm^{-1} 1715 (C=O).

2-{2-[2-(2-*Methacryloyloxyethoxy)ethoxy*]*ethoxy*}*ethyl* 3,4,-5-*Tris*(p-*dodecyloxybenzyloxy)benzoate* **5d**.—Compound **3f** (2.80 g, 2.4 mmol), methacryloyl chloride (0.93 cm^3, 9.6 mmol), and Et_3N (1.84 cm^3, 13.4 mmol) gave **5d** (2.05 g, 71%); purity 99% (HPLC); m.p. 51–52 °C; δ_H($CDCl_3$, TMS) 0.88 (t, 9 H, CH_3), 1.26 [overlapped peaks, 54 H, $(CH_2)_9$], 1.76 (overlapped peaks, 6 H, $CH_2CH_2OC_6H_4$), 1.93 (s, 3 H, $CH_3C{=}CH_2$), 3.64, 3.68 (overlapped peaks, 10 H, OCH_2CH_2O), 3.80 (t, 2 H, $C_6H_2CO_2CH_2CH_2$, *J* 4.3), 3.93 (overlapped peaks, 6 H, $CH_2OC_6H_4$), 4.28 [t, 2 H, $CH_2O_2CC(CH_3)$, *J* 5.1], 4.44 (t, 2 H, CH_2O_2CPh, *J* 4.3), 5.00 (s, 2 H, $OC_6H_4CH_2OC_6H_2CO_2$ from 4-position), 5.03 (s, 4 H, $OC_6H_4CH_2OC_6H_2CO_2$– from 3- and 5-positions), 5.55 [s, 1 H, $C(CH_3){=}CH_2$ *trans* to C=O], 6.11 [s, 1 H, $C(CH_3){=}CH_2$ *cis* to C=O], 6.75 (d, 2 H, $OC_6H_4CH_2OC_6H_2CO_2$– *o'*-H, *J* 8.4), 6.89 (d, 4 H, $OC_6H_4CH_2OC_6H_2CO_2$– *o*-H, *J* 8.8), 7.23 (d, 2 H, $OC_6H_4CH_2OC_6H_2CO_2$– *m'*-H, *J* 8.1), 7.32 (d, 4 H, $OC_6H_4CH_2OC_6H_2CO_2$ *m*-H, *J* 8.6) and 7.37 (s, 2 H, $C_6H_2CO_2$–); ν_{max}(KBr plate)/cm^{-1} 1715 (C=O).

Free-radical Polymerization of Compounds **5a–d**.—All polymerizations were carried out as described below for **5a**. In a dry Schlenk tube fitted with a rubber septum were placed **5a** (1.00 g, 0.90 mmol), 2,2'-azoisobutyronitrile (AIBN) (0.0030g, 0.018 mmol) and freshly distilled benzene (5.0 cm^3). The polymerization mixture was degassed by at least five freeze–pump–thaw cycles and then was stirred at 60 °C for 20–24 h. The polymer was purified by passing a light petroleum solution of it through a short column of neutral alumina, the unchanged monomer remaining on the column. This procedure yielded a white polymer (0.72 g, 72%) that was free of unchanged monomer as determined by GPC and ^{1}H NMR analyses.

Preparation of the Complexes of **3** *and* **6** with $LiCF_3SO_3$.—All complexes were made using the same procedure. In a vial were placed compounds **3** and **6** (0.050 g) and an appropriate volume (indicated below) of a solution of $LiCF_3SO_3$ in dry THF. All the solutions were then made up to the same volume with THF. The resultant solutions were then evaporated at room temperature under a partial vacuum (> 10 mmHg) for 24 h to afford the complexes which were further dried at 5×10^{-2} mmHg for 48 h at room temperature. An example is as follows. A THF solution (0.10 cm^3) containing $LiCF_3SO_3$ (6.93 mg, 4.44×10^{-3} mmol) was added to **3d** (0.050 g, 4.44×10^{-2} mmol) to yield 0.10 mol of $LiCF_3SO_3$ per mol of **3d**.

Results and Discussion

Lehn *et al.*[7] advanced the idea of constructing molecular channels from a tubular architecture which displays a columnar mesophase (*i.e.*, tubular mesophase) obtained from polysubstituted azamacrocyclic molecules. A large variety of similar and/or related systems displaying a columnar hexagonal mesophase were subsequently reported.[8–11] The polysubstitution of azamacrocyclic molecules was accomplished by their esterification with *p*-(alkyloxy)benzoic acid,[7–11] 3,4-bis(*p*-alkyloxy)benzoic acid,[9c,10c,d] and with 3,4,5-tris(*p*-alkyloxy)-benzoic acid.[10d]

Both 3,4,5-tris(*p*-alkyloxy)benzoic acid and 3,4,5-tris(*p*-alkyloxybenzylozy)benzoic acid are flat molecules which resemble a triangular layered architecture which can be used in the construction of cylindrically shaped architectures which display a columnar hexagonal mesophase.[2,3,12,13]

Scheme 1 outlines the synthesis of the novel tapered structural units **3a–f** which are derived from 4'-methyl(benzo-15-crown-5)-3,4,5-tris(*p*-dodecyloxybenzyloxy)benzoate in which the selective benzo-15-crown-5 *endo*-receptor was replaced with the non-selective *endo*-receptors based on oligo-(oxyethylene) segments of different length (*i.e.*, degrees of oligomerization from 1 to 4). The synthesis of compounds **3a–g** was performed by an esterification performed under mildly basic reaction conditions as described in the Experimental section. Its mechanism will be discussed in a separate publication.[14]

Fig. 1 shows the ^{1}H NMR spectrum of **3d** together with its protonic assignments which is a representative example for compounds **3**. All benzylic and aromatic resonances of the external *p*-alkoxybenzyl ether groups are downfield from those of the internal *p*-alkoxybenzyl ether group. The signals at 6.89 (e) and 7.33 ppm (f) and that at 5.05 (g) are associated with the aromatic and benzylic protons of the *p*-alkoxybenzyl ether groups from the 3 and 5 positions of the gallic ester, respectively, while the resonances of the corresponding *p*-alkoxybenzyl ether group from the 4 position are at 6.75 (e'), 7.24 (f') and 5.00 (g'), respectively. The shielding effect of the phenylenic units affects also the resonances of the CH_2 groups located in the α position of the alkyloxy groups [overlapped triplets at 3.95 (d) and 3.91 ppm (d')].

Compounds **3b**, **e** and **3g** were used as models for the other low molecular weight derivatives and for their polymers. The methacrylates **5a–d** were synthesized by the esterficiation of **3a**, **c**, **d** and **f** with methacryloyl chloride. Polymers **6a–d** were obtained by the radical polymerization of the monomers **5a–d** initiated with AIBN in benzene at 60 °C.

The phase behaviour of the compounds **3a–f** and **6a–d** was determined by a combination of techniques consisting of DSC, thermal optical polarized microscopy, and X-ray scattering experiments. The X-ray scattering experiments will be discussed in the second part of this paper. The DSC traces of first heating [Fig. 2(*a*)], first cooling [Fig. 2(*b*)], and second heating scans [Fig. 2(*c*)] of **3a, c, d, f** and **6a–d** are shown in Fig. 2. The phase transition temperatures and the associated enthalpy changes of **1**, **3** and **6** are presented in Table 1. With the exception of the model methoxy functional compounds **3b**, **3e** and of the dimer **3g**, all other compounds exhibit an enantiotropic hexagonal columnar (Φ_h) mesophase which was confirmed by X-ray scattering experiments. The dimer **3g** displays a monotropic Φ_h phase with an isotropization transition temperature (T_i) lower than that of its corresponding monomer **3**. Compounds **3b** and **3e** are analogous to **3a** and **3d** except that the hydroxy functionality was replaced with a methoxy group. The latter has the effect of removing the possibility of hydrogen bonding occurring either intra- or intermolecularly. Table 1 shows that in the absence of hydrogen bonding only the dimer **3g** forms a Φ_h mesophase which is, however, monotropic. Compound **3g** represents a model of two molecules of **3c** that are covalently bonded together. With the absence of hydrogen bonding and the additional positional restrictions placed by the covalent attachment of the two groups, **3g** does not form an enantiotropic Φ_h mesophase and its isotropic Φ_k transition temperature is lower than that of **3c**

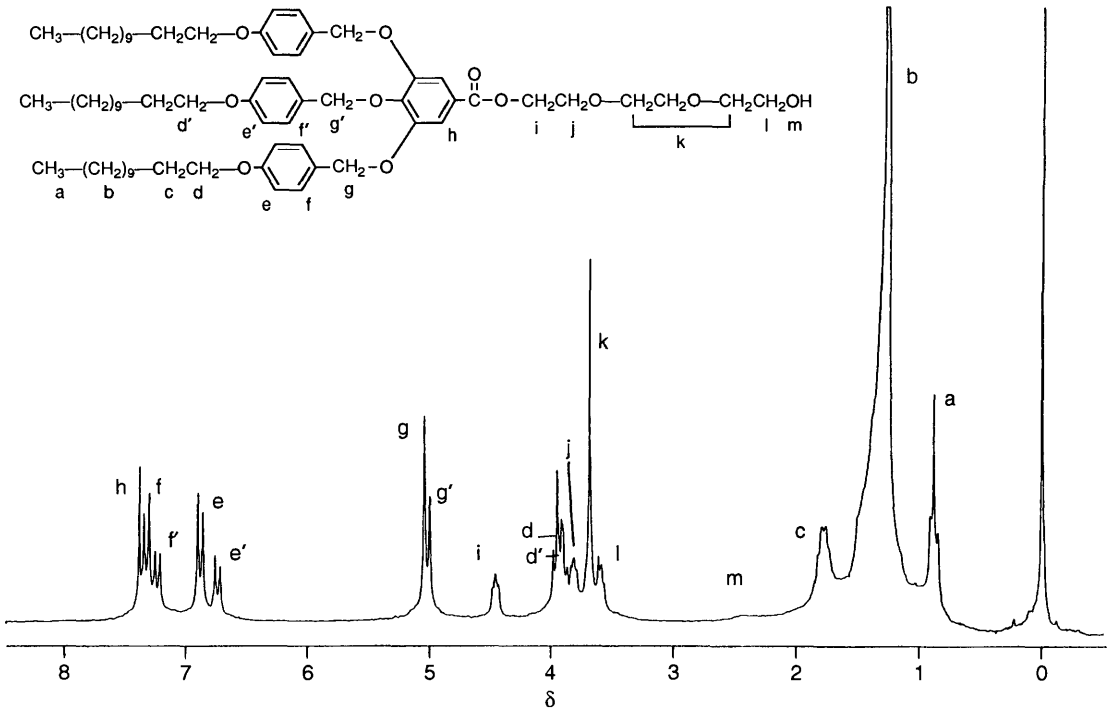

Fig. 1 200 MHz ^{1}H NMR spectrum of **3d** ($CDCl_3$, TMS)

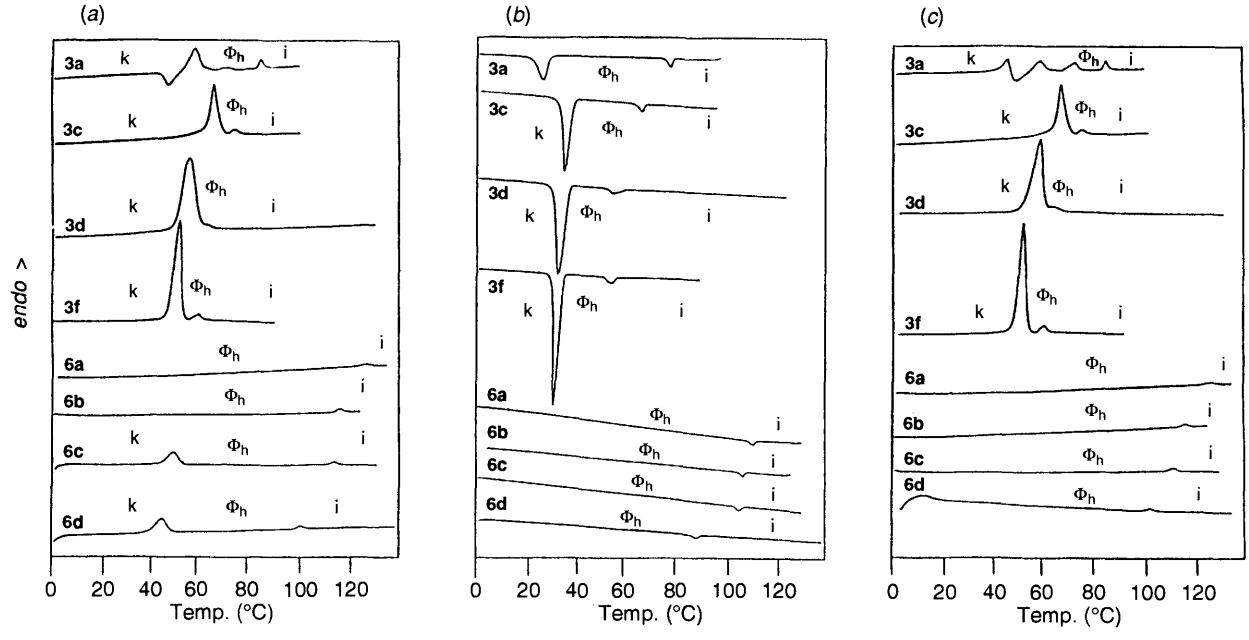

Fig. 2 DSC traces (20 °C/min^{-1}) of **3a**, **3c**, **3d**, **3f** and **6a–d** recorded during (a) first heating, (b) first cooling and (c) second heating scans

(Table 1). Therefore, the presence of the OH group in the monomer **3c** enhances both the stability of the Φ_h phase and its enantiotropic character more than its dimerization does. The phase behaviour of **1** was discussed in a previous publication.[6] Compounds **3a**, **c**, **d**, **f** and **6c**, **d** form lamellar crystalline phases. The transition temperatures of compounds **3** and **6** determined from the first heating scan are plotted *versus* the number of OE segments present in the molecule in Fig. 3(*a*). T_i of the Φ_h mesophase of compounds **3a**, **c**, **d** and **f**, decreases as the number of OE segments present in the flexible *endo*-receptor increases. Concurrently, the melting temperature (T_m) is also suppressed. Polymers **6a–d** also show a decrease of T_i and T_m with increasing the number of OE segments. Polymers **6a** and **6b** do not exhibit a crystalline phase within this range of temperatures. Nevertheless, in all cases, T_i of the polymers is 45 °C higher on heating and 35 °C lower on cooling than that of the corresponding monomers **3** (Table 1). The difference between heating and cooling is due to the higher supercooling of the T_i in the polymers *versus* that of the monomers.

Fig. 3(*b*) shows the dependence of the enthalpy changes associated with the isotropic Φ_h phase transition ($\Delta H_{i-\Phi h}$) determined from the DSC cooling scan, *versus* the number of OE segments in the *endo*-receptor. Compounds **3a**, **c**, **d** and **f** show very little change of the $\Delta H_{i-\Phi h}$ as a function of the number of OE segments. Nevertheless, these enthalpy changes seem to first decrease and then increase with the increase of the number of OE units. The polymers **6** do, however, show a clear increase of their $\Delta H_{i-\Phi h}$ as the number of OE segments increases. Therefore, the dependence of the $\Delta H_{i-\Phi h}$ *versus* the number of OE units is just opposite to that of the corresponding

Table 1 Characterization of compounds **1**, **3a–g**, and **6a–d** (Φ_h = hexagonal columnar mesophase; k = crystalline phases; i = isotropic phase). Data on the first line are from the first heating and cooling scans and data on the second line are from the second heating scans

Compd.	Yield (%)	Purity (%)	GPC $M_n \times 10^{-3}$	GPC M_w/M_n	Thermal transition (°C) and corresponding enthalpy (kcal mru^{-1})/ entropy (cal mru^{-1} K^{-1}) changes in parentheses: Heating	Cooling
1	60	99	—	—	k 49 (1.3) k 73 (14.2) Φ_h 147 (3.1/7.4) i	i 137 (3.0/7.3) Φ_h 51, 41 (6.9)[a] k 9 (0.58) k
					k 17 (0.77) k 49, 62, 71 (6.92)[a] Φ_h 143 (2.89/6.9) i	
3a	68	99	—	—	k 46 (1.8) 8 58 (4.9) k 61 (0.39) Φ_h 85 (0.73/2.0) i	
					k 45 (1.8) k 48 (−1.1) k 56 (2.1) k 72 (1.2) Φ_h 84 (0.73/2.0) i	i 76 (0.76/2.2) Φ_h 25 (4.2) k
3b	31	99	—	—	k 53 (18.97) i	
					k 52 (17.17) i	i 32 (16.56) k
3c	48	99	—	—	k 66 (8.3) Φ_h 73 (0.70/2.0) i	
					k 66 (8.3) Φ_h 73 (0.72/2.1) i	i 65 (0.74/2.2) Φ_h 35 (9.5) k
3d	69	99	—	—	k 56 (18.9) Φ_h 63 (0.80/2.4) i	
					k 56 (13.3) Φ_h 61 (0.75/2.2) i	i 54 (0.72/2.2) Φ_h 34 (14.7) k
3e	19	99	—	—	k 43 (13.9) k 52 (4.9) i	
					k 46 (17.5) i	i 28 (17.2) k
3f	63	99	—	—	k 50 (16.4) Φ_h 59 (0.74/2.2) i	
					k 49 (15.5) Φ_h 57 (0.77/2.3) i	i 52 (0.78/2.4) Φ_h 31 (15.1) k
3g	13	99	—	—	k 63 (25.0) i	
					k 66 (20.9) i	i 55 (1.1/3.4) Φ_h 23 (19.6) k
6a	72	99	27.7	2.1	Φ_h 127 (0.36/0.9) i	
					Φ_h 127 (0.36/0.9) i	i 110 (0.38/1.0) Φ_h
6b	44	99	24.6	1.7	g 36 Φ_h 116 (0.41/1.1) i	
					g 37 Φ_h 116 (0.38/1.0) i	i 103 (0.38/1.0) Φ_h 29 g
6c	70	99	44.7	2.3	k 48 (3.32) Φ_h 113 (0.43/1.1) i	
					Φ_h 112 (0.43/1.1) i	i 103 (0.45/1.2) Φ_h
6d	68	99	69.1	2.5	k 47 (3.75) Φ_h 103 (0.50/1.3) i	
					Φ_h 99 (0.43/1.2) i	i 87 (0.50/1.4) Φ_h

[a] Combined enthalpies for overlapped peaks.

Table 2 Thermal transitions of the complexes of **3d** and **6c** with various amounts of added $LiCF_2SO_3$ (Φ_h = hexagonal columnar mesophase; k = crystalline phases; i = isotropic phase). Data on the first line are from the first heating and cooling scans and data on the second line are from the second heating scans

$LiCF_3SO_3$ (mol)	Thermal transition (°C) and corresponding enthalpy changes (kcal mru^{-1})[a] in parentheses: **3d** Heating	**3d** Cooling	**6c** Heating	**6c** Cooling
0.00	k 56 (18.9) Φ_h 63 (0.80) i	i 54 (0.72) Φ_h 34 (14.7) k	k 48 (3.32) Φ_h 113 (0.43) i	i 103 (0.45) Φ_h
	k 56 (13.3) Φ_h 61 (0.75) i		Φ_h 112 (0.43) i	
0.10	k 58 (13.6) Φ_h 73 (0.72) i	i 55 (0.46) Φ_h 27 (12.2) k	Φ_h 116 (0.57) i	i 105 (0.47) Φ_h
	k 53 (13.3) Φ_h 64 (0.68) i		Φ_h 115 (0.50) i	
0.20	k 56 (13.4) Φ_h 84 (0.51) i	i 76 (0.54) Φ_h 32 (13.7) k	Φ_h 123 (0.39) i	i 111 (0.35) Φ_h
	k 56 (14.1) Φ_h 83 (0.57) i		Φ_h 122 (0.32) i	
0.30	k 54 (13.6) Φ_h 90 (0.52) i	i 82 (0.47) Φ_h 30 (13.1) k	k 52 (0.27) Φ_h 117 (0.21) i	i 116 (0.28) Φ_h
	k 54 (13.8) Φ_h 89 (0.50) i		Φ_h 124 (0.22) i	
0.40	k 43, 54 (16.9)[b] Φ_h 99 (0.48) i	i 89 (0.43) Φ_h 28 (13.3) k	k 48 (0.29) Φ_h 122 (0.19) i	i 118 (0.22) Φ_h
	k 54 (13.4) Φ_h 97 (0.40) i		Φ_h 129 (0.14) i	
0.50	k 52 (13.8) Φ_h 105 (0.47) i	i 97 (0.29) Φ_h 30 (12.5) k	k 55 (0.50) Φ_h 118 (0.17) i	i 113 (0.09) Φ_h
	k 52 (12.9) Φ_h 103 (0.38) i		Φ_h 126 (0.05) i	
0.60	k 51 (12.9) Φ_h 111 (0.26) i	i 102 (0.25) Φ_h 30 (11.9) k		
	k 52 (12.4) Φ_h 108 (0.33) i			
0.70	k 52 (12.5) Φ_h 115 (0.11) i	i 106 (0.22) Φ_h 29 (11.3) k		
	k 52 (12.1) Φ_h 113 (0.27) i			
0.80	k 53 (12.2) Φ_h 123 (0.24) i	i 109 (0.30) Φ_h 28 (10.4) k		
	k 53 (11.1) Φ_h 117 (0.27) i			
0.90	k 52 (11.9) Φ_h 128 (0.22) i	i 110 (0.26) Φ_h 25 (7.8) k		
	k 16 (0.18) k 50 (9.1) Φ_h 115 (0.24) i			
1.00	k 52 (12.2) Φ_h 134 (0.24) i	i 97 (0.12) Φ_h 21 (5.1) k		
	k 14 (0.34) k 26 (−0.64) k 47 (6.4) Φ_h 106 (0.14) i			
1.20	k 51 (11.6) Φ_h 138 (0.09) i	i 62 (0.06) Φ_h 13, 0 (1.3)[b] k		
	k 13 (1.5) k 27 (−1.4) k 46 (2.7) Φ_h 74 (0.10) i			

[a] The molecular weight is weight averaged with the amount of $LiCF_3SO_3$ present in the complex. [b] Combined enthalpies for overlapped peaks.

T_i. In addition, the $\Delta H_{i-\Phi h}$ of the monomers **3** are about twice as large as those of the corresponding polymers **6** (Table 1, Fig. 3b). This trend is again opposite to that of the T_i of the monomers *versus* that of the corresponding polymers (Table 1, Fig. 3a).

Both monomers **3** and polymers **6** dissolve metal salts and form stable complexes which maintain the Φ_h mesophase up to higher temperatures than those of the individual pure compounds. Upon sequential addition of $LiCF_3SO_3$, **3d** and **6c**

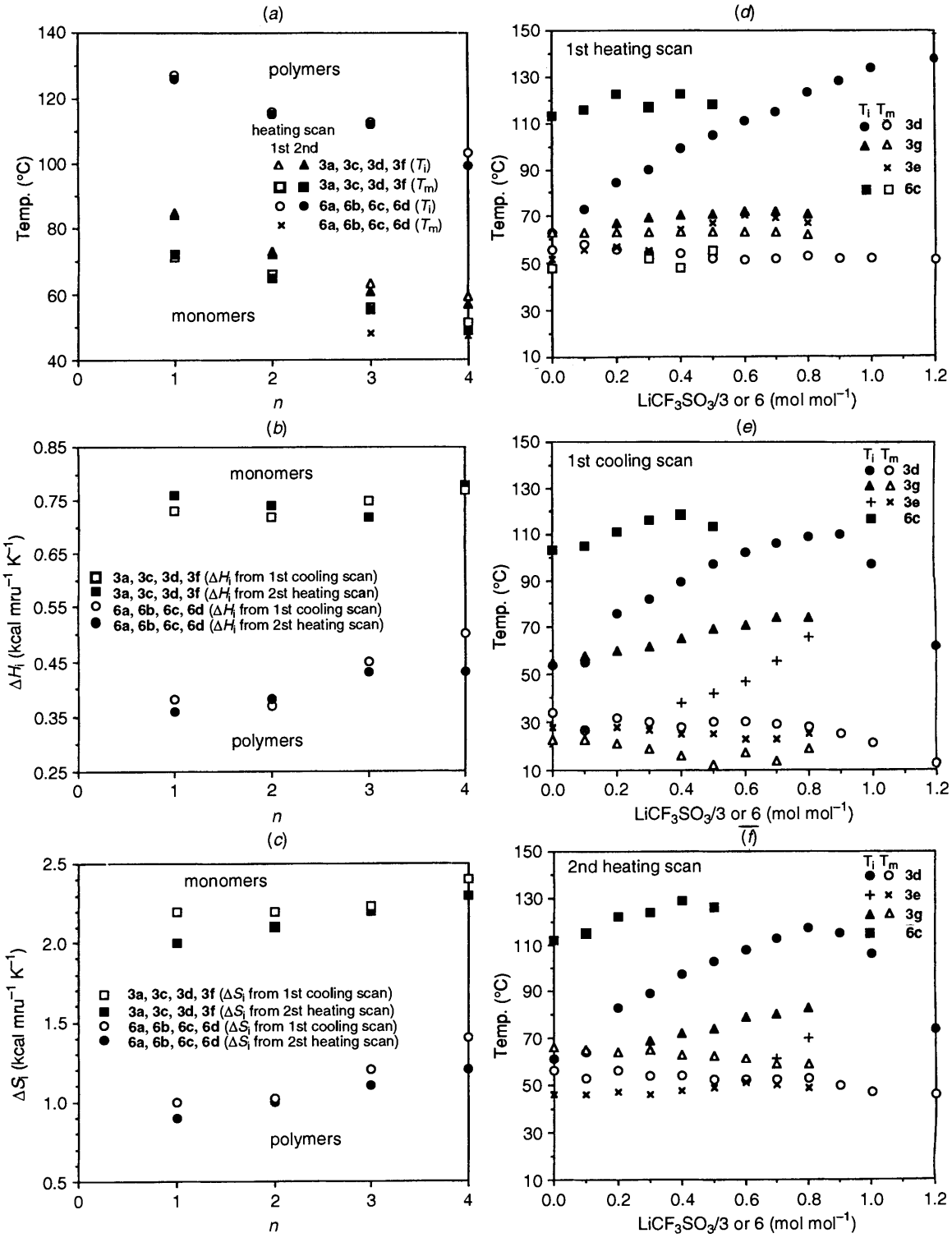

Fig. 3 (*a*) The dependence of: k–Φ_h (□, ■) and Φ_{h-i} (△, ▲) phase transition temperatures of **3a**, **c**, **d**, **f**, and of k–Φ_h (×) and Φ_{h-i} (○, ●) phase transition temperatures of the corresponding polymers **6d**–**d** *versus* the number of oxyethylene segments (*n*) in the *endo-receptor*. Φ_h-Isotropization temperature from first heating (open symbols) and second heating (filled symbols) DSC scans; (*b*) the dependence of: enthalpy change (ΔH_i) associated with Φ_{h-i} (□, ■) phase transition of **3a**, **c**, **d**, **f**, and of the Φ_{h-i} (○, ●) phase transition of the corresponding polymers **6a**–**d** *versus n* from first cooling (open symbols) and second heating (filled symbols) DSC scans; (*c*) The dependence of: entropy change (ΔS_i) associated with Φ_{h-i} (□, ■) phase transition of **3a**, **c**, **d**, **f**, and of the Φ_{h-i} (○, ●) phase transition of the corresponding polymers **6a**–**d** *versus n* from first cooling (open symbols) and second heating (filled symbols) DSC scans; and the dependence of the k–Φ_h (T_m, open symbols) and Φ_{h-i} (T_i, closed symbols) phase transition temperatures of the complexes of **3d** (○, ●), **3g** (△, ▲), **3e** (+, ×), and **6c** (□, ■) with various amounts of $LiCF_3SO_3$ (Table 2 and unpublished data) from the data of (*d*) the first heating scans; (*e*) the first cooling scans; (*f*) the second heating scans.

exhibit a continuous increase in the $T_{\Phi h-i}$. DSC traces of **3d** are shown in Fig. 4 and the phase transition temperatures of the complexes of **3d** and **6c** with various amounts of $LiCF_3SO_3$ are presented in Table 2. The T_m of the complexes of **3d** decreases very little with increasing $LiCF_3SO_3$ concentration while the $T_{\Phi h-i}$ increases sharply in the first heating scan [Fig. 4(*a*), Table 2]. However, both ΔH of melting and isotropization decrease with the increased amount of $LiCF_3SO_3$ in the

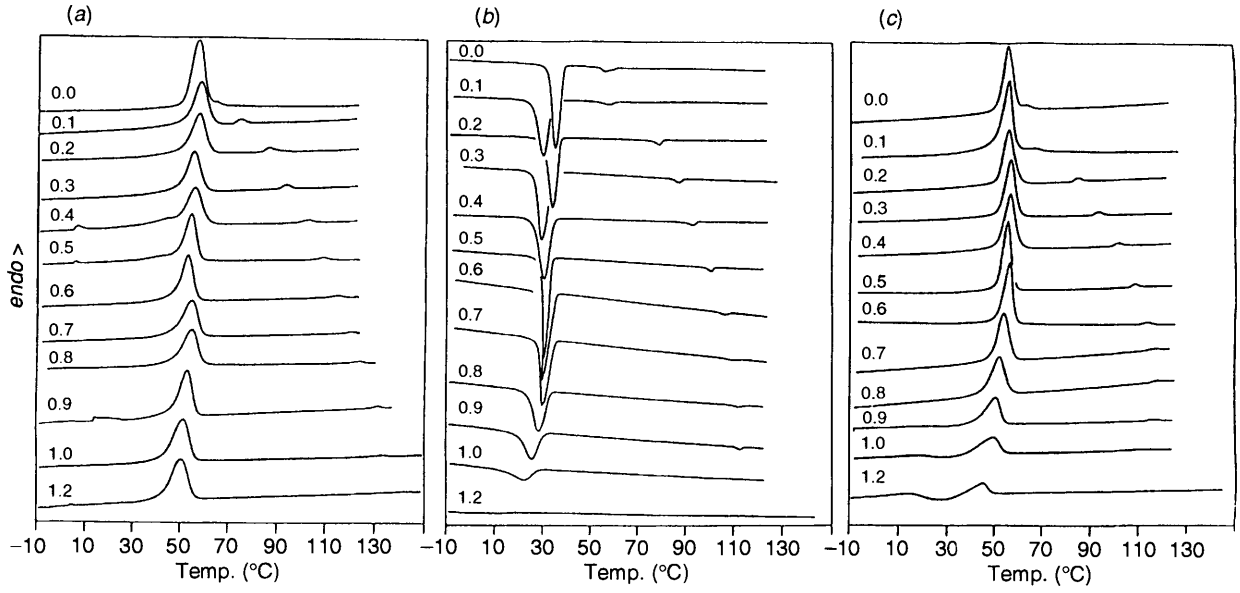

Fig. 4 DSC traces (20 °C min^{-1}) of the complexes of **3d** with $LiCF_3SO_3$: recorded during (a) first heating; (b) first cooling; (c) second heating scans

complexes of **3d**. This trend is also observed on the cooling [Fig. 4(*b*)] and on the second heating scans [Fig. 4(*c*), Table 2] until a concentration of 0.8 mol equiv. of $LiCF_3SO_3$ per mol equiv. of **3d** is reached. Above this concentration the isotropization endotherm broadens and a shift to lower temperatures of both the Φ_{h-i} and k–Φ_h transitions is observed in the first cooling and second heating scans. In order to understand this behaviour, a sample of **3d** containing 2.0 mol equiv. of $LiCF_3SO_3$ was annealed at 200 °C for 5 min and then analysed by ^1H NMR spectroscopy. The signals associated with the phenyl benzyl ether bonds ($PhCH_2OPh$) at 5.00 and 5.05 ppm were absent. Therefore, thermal decomposition of the tapered group occurred at elevated temperatures, most likely, resulting from the Lewis acid character of the $LiCF_2SO_3$ salt.[15]

The changes in the phase behaviour that occurs for the polymer **6c** upon complexation with $LiCF_3SO_3$ is less substantial and not as systematic as that seen with **3d** [Table 2, Fig. 3(*d*, *e*, *f*)]. Up to a concentration of 0.4 mol equiv. of $LiCF_3SO_3$ the complexes of **3d** show an increase of their Φ_{h-i} of up to 36 °C whereas the complexes of polymer **6c** show an increase of only 16 °C. Above 0.5 mol equiv. of $LiCF_3SO_3$ the complexes of **6c** appear to show a more complicated behaviour possibly resulting from the decomposition of the phenyl benzyl ether bonds as was seen in the case of **3d**. The complexes of **3e** with up to 0.3 mol equiv. of $LiCF_3SO_3$ per monomer unit are only crystalline [Fig. 3(*d*, *e*, *f*)]. Above this concentration, these complexes form also a monotropic Φ_h phase. Above 0.4 mol equiv. of salt per monomer repeat, the $T_{i-\Phi h}$ of the complexes of **3e** with $LiCF_3SO_3$ follows the same trend with that of the complexes of **3d** except that T_i of the complexes of **3e** is about 50 °C lower. The complexes of the dimeric compound **3g** with $LiCF_3SO_3$ follow a similar trend (*i.e.*, the slope of the $T_{i-\Phi h}$ *vs.* salt content) with those of the polymer **6c** [Fig. 3(*d*–*f*)]. However, the $T_{i-\Phi h}$ of the complexes of **3g** is lower than both that of the polymer **6c** and of the monomer **3d** and, subsequently, can be assumed to be lower than that of the complexes of **3c** and **6b**. A more detailed discussion on these and their salt complexes will be presented elsewhere.

Representative examples of the textures of the Φ_h mesophases exhibited by **3d**, a complex of **3d** with 0.5 mol equiv. of $LiCF_3SO_3$ and of **6c** are presented in Fig. 5.

Compounds **3a**, **c**, **d**, **f**, **g**, **6a**–**d** and the complexes of **3d** with 0.7 and 1.0 mol equiv. of $LiCF_3SO_3$ were characterized by small and wide angle X-ray scattering. The complexes of **3a**, **c**, **d**, **f**, **g** and **3d** with 0.7 and 1.0 mol equiv. of $LiCF_3SO_3$ were characterized in their Φ_h mesophase. Compounds **6a**–**d** were characterized at both 25 °C and at higher temperature in the Φ_h mesophase with the exception of **6c** which was characterized only at 25 °C in the Φ_h mesophase. The d spacings of all reflections are presented in Table 3 together with the measured column radius (R). In their Φ_h mesophase, compounds **3a** **c**, **d**, **f**, **g** and **6a**, **b** and **d** have X-ray reflections in the ratio: $d_0:f_1:d_2 = 1:1/\sqrt{3}:1/2$, with only a diffuse scattering at wide angles. This is indicative of a hexagonal columnar (Φ_h) mesophase.[2,3,16]

Fig. 6a shows the dependence of the column radius of the self-assembled tubular structures as a function of the number of OE segments present in the molecule of **3a**, **c**, **d**, **f**, **g**, or structural unit of **6a**, **b**, **c**, **d**. The column radius increases with the number of OE units in the molecule. The polymers **6** have a radius that is about 2 Å larger than that of their low molecular weight homologous compounds **3**. The dependence of the column radius of **3d** on the amount of $LiCF_2SO_3$ present in the complex is shown in Fig. 6(*b*). The addition of salt induces a small increase in the column radius.

Table 3 also summarizes the experimental densities (ρ) of all compounds. From the experimental value of the distance from the column centre to the hexagon vertex S and the experimental densities (ρ) we can calculate the number of molecules of **3** or repeat units of **6** that are present in a hexagonal prism layer (μ) with a height of 3.74 Å:[3,17]

$$\rho = \frac{2\mu M}{3\sqrt{3}N_A S^2 t}$$

Here M is the molecular weight of **3** or **6**, μ is the number of molecules of **3** or **6** in a cross-section, N_A is 6.022 045 × 10^{23} (Avogadro's number). The details of this calculation have been presented in a previous paper.[3] Values of μ are listed in the final column of Table 3. Based on these calculations **3a** and **c** have about **4** molecules per layer, and **3d** and **3f** have 5.4 and 5.1 molecules per layer respectively. Polymer **6a** has 4.5 repeat units per layer, **6b** has 5.1, while **6c** and **6d** have 5.9 repeat units per layer.

With the increasing number of OE units in the molecule, the number of molecules that are required per layer increases. There is an increase of the number of repeat units per layer for the polymer as compared to the number of low molecular weight alcohols **3** containing the same number of OE segments.

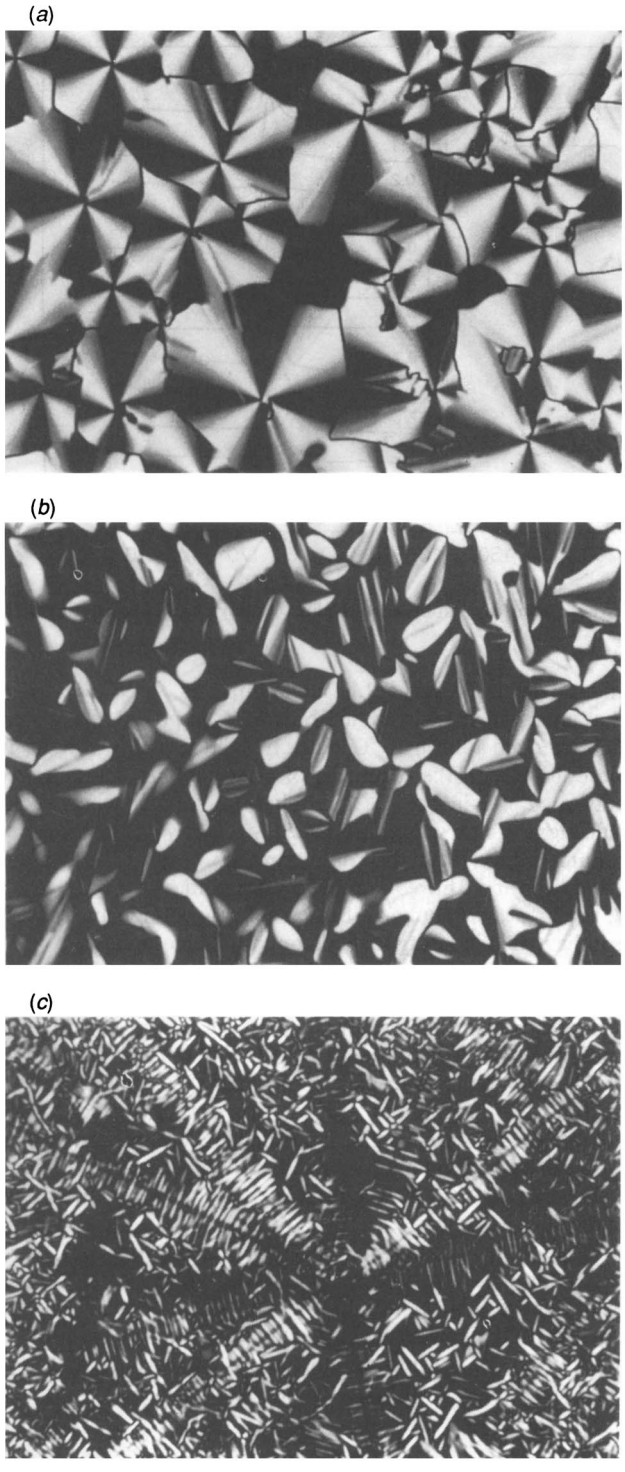

Fig. 5 Representative optical polarized micrographs of the texture exhibited by the hexagonal columnar (Φ_h) mesophase of: (*a*) **3d** upon cooling from 72 °C to 58 °C (1 °C min^{-1}); (*b*) the complex of **3d** with 0.5 mol equiv. of $LiCF_3SO_3$ upon cooling from 107 °C to 99 °C (1 °C min^{-1}); (*c*) **6c** upon cooling from 115 °C to 93 °C (0.1 °C min^{-1})

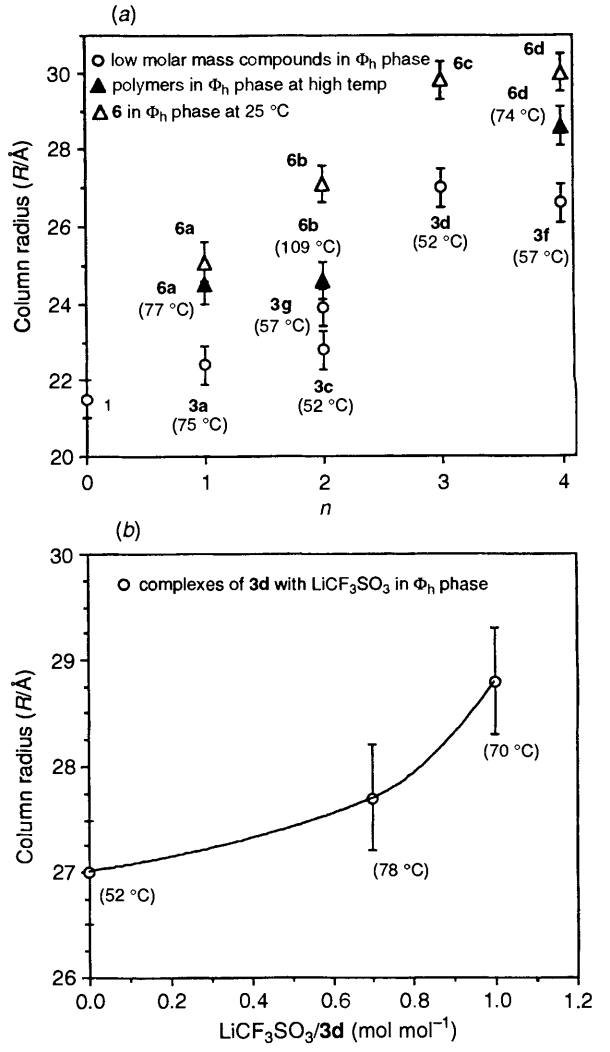

Fig. 6 The dependence of the column radius in the Φ_h phase of: (*a*) **3a, c, d, f, g** (○), and of **6a, b, d** (▲) at high temperatures and of **6a–d** (△) in the Φ_h phase at room temperature (data from Table 3); (*b*) of the complexes of **d** (○) with various amounts of $LiCF_3SO_3$ in the Φ_h phase (data from Table 3)

Using a molecular modelling program we have constructed a schematic model of a stratum of the column formed by **3d** (Fig. 7) and **6c** (Fig. 8) as well as the side views of five of these layers stacked on top of each other and forming a cylinder. Fig. 7 shows the molecules of **3d** with the hydroxy-terminated OE segments pointing to the centre of the column and the wider aliphatic tail part of the tapered molecule pointing towards the periphery of the column. Fig. 7(*a*) shows the alkyl tails fully extended, while Fig. 7(*b*) shows the alkyl tails melted so that the model cross-section corresponds to the average cross-section determined by the X-ray diffraction. This arrangement resembles that of the inverse micelle in the lyotropic hexagonal phase.[18] Only a cross-section is shown in the top views. The hydroxy-terminated OE segments in this model are able to participate in H-bonding and dipolar attractive interactions, while the alkyl tails are concentrated at the periphery due to hydrophobic interactions. This combination of polar and non-polar regions within the same molecule leads to aggregation *via* microsegregation. Above T_m, these molecules self-assemble into cylinders which pack in a hexagonal arrangement producing the observed Φ_h liquid crystalline mesophase.

Similarly, the model of the polymer **6c** with the alkyl tails melted in order to correspond to the average radius measured is presented in Fig. 8(*a*) and 8(*b*), respectively. The polymers **6** have the terminal hydroxy group of the OE segment replaced with a covalent bond to a polymethacrylate backbone. Any H-bonding interactions that may occur in **3d** from Fig. 7 are absent in the polymer **6c** from Fig. 8. In addition, positioning the repeat units in a cylindrical fashion while maintaining the experimentally determined number of tapered units per stratum (μ, Table 3) becomes more difficult as a result of the positional restrictions that arise from the covalent attachment to the polymer backbone. Fig. 6(*a*) shows the resultant increase in column diameter that occurs when the tapered groups are bonded to the polymer backbone in compounds **6** compared

Table 3 Characterization of the Φ_h phase of compounds **3** and **6** by small-angle X-ray scattering

Compd.	Temp. (°C)	d_{100} (Å)	d_{110} (Å)	d_{200} (Å)	$\langle d_{100}\rangle$[a] (Å)	Lattice parameter a[b] (Å)	R[b] (Å)	S[b] (Å)	(R + S)/2 (Å)	ρ[c] (g cm^{-3})	μ[d]
3a	75	38.5	22.5	19.0	38.8	44.8	22.4	25.9	24.2	1.061	4.0
3c	67	39.4	22.8	19.9	39.5	45.6	22.8	26.3	24.6	1.040	3.9
3d	52	46.4	27.1	23.1	46.8	54.0	27.0	31.2	29.1	1.068	5.4
3d + 0.7 mol of $LiCF_3SO_3$	78	47.2	27.6	23.9	47.9	55.3	27.7	32.0	29.9		
3d + 1.0 mol of $LiCF_3SO_3$	70	48.7	28.2	24.6	49.1	56.7	28.3	32.7	30.5		
3f	54	46.1	26.8	23.0	46.1	53.2	26.6	30.7	28.7	1.071	5.1
3g	57	40.5	23.6	20.2	41.4	47.8	23.9	27.6	25.8	1.032	2.1
6a	77	42.7	25.2	20.7	42.5	49.0	24.5	28.3	26.4		
6a	25	44.0	24.9	21.7	43.5	50.2	25.1	29.0	27.1	1.008	4.5
6b	109	42.7	—[e]	—[e]	42.7	49.3	24.6	28.4	26.5		
6b	25	47.1	27.1	23.3	46.9	54.1	27.1	31.3	29.2	1.016	5.1
6c	25	52.0	30.0	25.6	51.8	59.8	29.9	34.5	32.2	1.002	5.9
6d	74	50.5	28.3	24.6	49.5	57.2	28.6	33.0	30.8		
6d[f]	25	52.0	29.8	26.0	52.0	60.0	30.0	34.6	32.3	1.049	5.9

[a] $\langle d_{100}\rangle = (d_{100} + d_{110} \times \sqrt{3} + d_{200} \times 2)/3$. [b] $a = 2\langle d_{100}\rangle/\sqrt{3}$, $R = \langle d_{100}\rangle/\sqrt{3}$, $S = 2 \times R/\sqrt{3}$. [c] ρ = experimental density at 20 °C. [d] μ = number of monomer units per column stratum. [e] Reflections are very weak. [f] The additional reflection d_{210} = 19.8 Å.

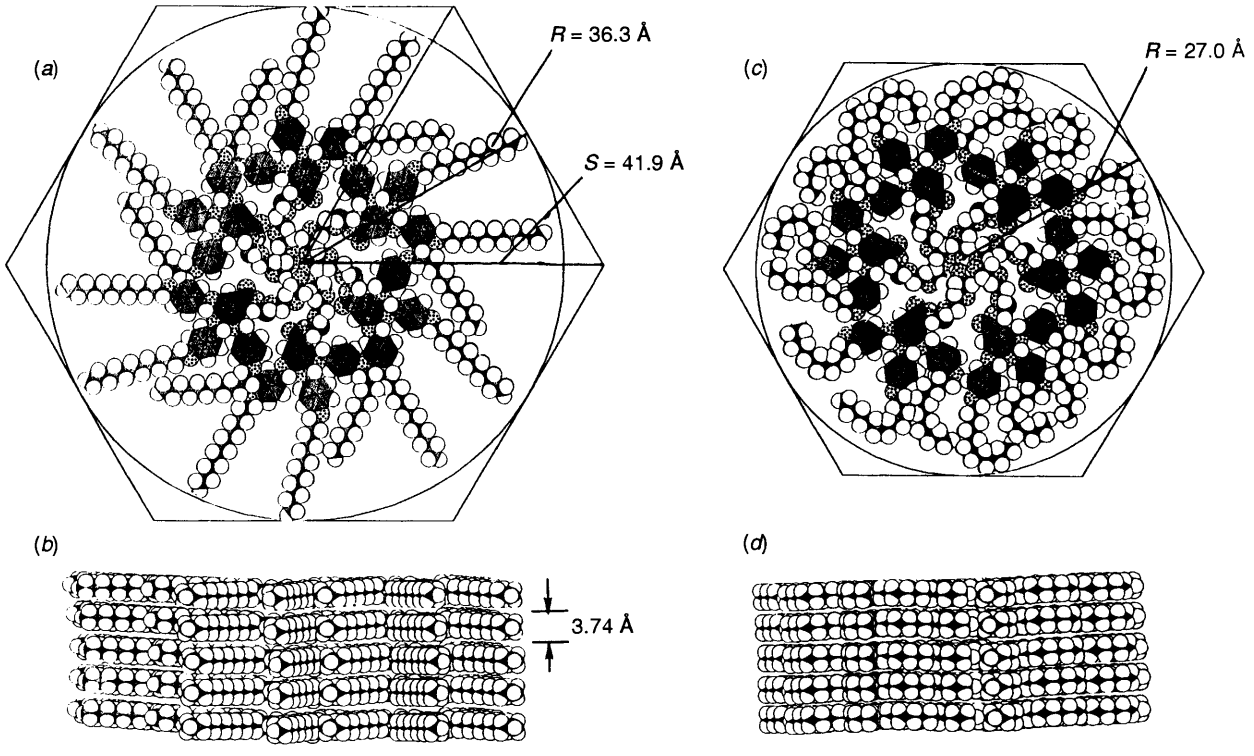

Fig. 7 Schematic representation of the supramolecular cylinders of **3d** in the Φ_h mesophase: (*a*) top view of the cylinder containing 6 molecules of **3d** in a stratum; (*b*) side view of a column containing 5 strata from Fig. 7(*a*); (*c*) top view of the cylinder containing 6 molecules of **3d** in a stratum with the alkyl tails melted to match the average column radius determined by X-ray scattering experiments; (*d*) side view of a column containing 5 strata from Fig. 7(*c*)

to the self-assembled compounds **3** that lack the positional restrictions imposed by the polymer backbone.

Fig. 3(*a*) shows the effect of the polymer backbone on the crystalline and liquid crystalline phases. Both the low molecular weight compounds **3** and their polymeric analogues **6** show similar decrease in the T_i with the increasing number (n) of OE segments. The only difference is that the replacement of the hydroxy functionality with covalent attachment to the polymer backbone results in an increase of the T_i of the polymers by an average of 45 °C. The T_i of both the polymer and monomer decreases with increasing number of OE units. With notable exceptions, this follows the usual trend for liquid crystals containing flexible tails or spacer moieties.[19] This trend has been also confirmed for discotic columnar phases.[20] In the case of the monomers we note that ΔH_i is almost independent of n and since $T_i = \Delta H_i/\Delta S_i$, the change in T_i is mostly attributable to the increase in ΔS_i [Fig. 3(*c*)]. In the case of the polymer, ΔH_i increases with n [Fig. 3(*b*)]. However, the decrease in T_i [Fig. 3(*a*)] implies that this is overcompensated by an even larger increase in ΔS_i [Fig. 3(*c*)]. A qualitative interpretation for this larger increase in ΔS_i in the case of the polymer could be sought in considering the configurational entropy of the OE spacer linking the tapered unit to the polymer backbone. This entropy is likely to be the lower the shorter the spacer and the more

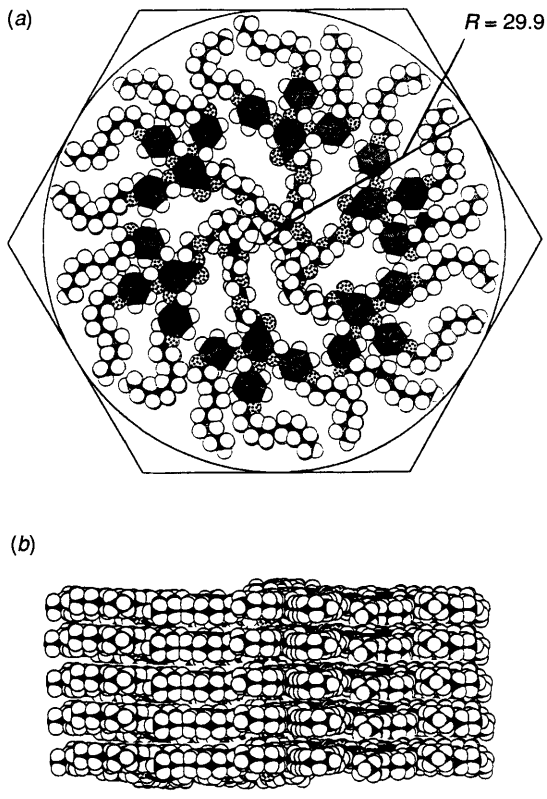

Fig. 8 Schematic representation of the supramolecular cylinders of **6c** in the Φ_h mesophase: (*a*) top view of a cylinder of **6c** containing 6 repeat units in a stratum with the alkyl tails melted to match the average column radius determined by X-ray scattering experiments; (*b*) side view of a cylinder of **6c** containing 30 repeat units of the polymer assembled with melted alkyl tails

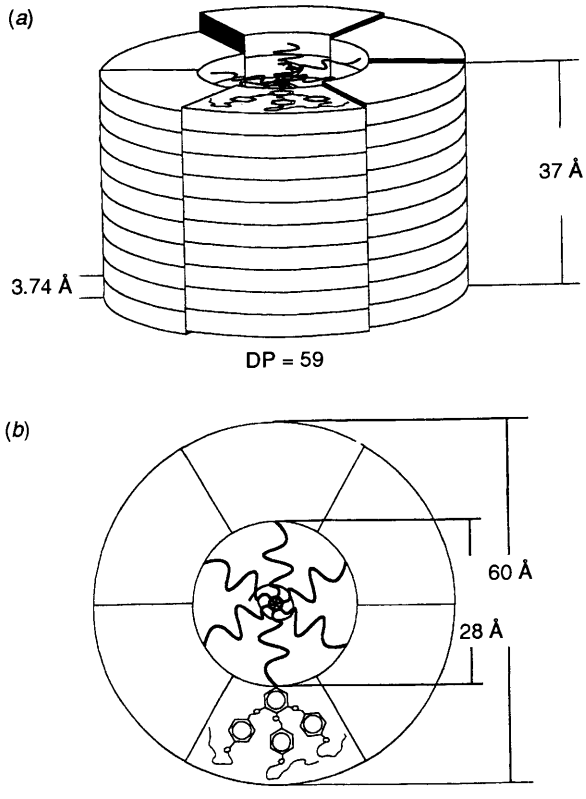

Fig. 9 An idealized representation of the supramolecular cylinder self-assembled from a single chain of **6d** in the hexagonal columnar phase, assuming one single backbone per cylinder, drawn to proportion with existing experimental data: (*a*) tilted side view; (*b*) top view

restricted the backbone is. We suggest that it is the conformational restriction of the backbone in the Φ_h phase which is responsible for the particularly low entropy of polymers with short spacers (*e.g.* **6a**) in the Φ_h phase, and thus in turn for the larger increase in ΔS_i with increasing *n*.

At this point, we can make for the first time a qualitative comparison between a 'molecular' polymethacrylate backbone and a 'supramolecular' backbone generated by a combination of H-bonding and ionic interactions. This can be done by comparing $T_{\Phi h-i}$ values of the monomer **3d** (T_m = 56 °C, $T_{\Phi h-i}$ = 63 °C), model **3e** (T_m = 46 °C), polymer **6c** (T_m = 48 °C, $T_{\Phi h-i}$ = 113 °C) [Table 1, Fig. 3(*d*, *e*)] and of the complexes of **3d** and **3e** with $LiCF_3SO_3$ (Table 2, Fig. 4d). About 0.85 mol equiv. of $LiCF_2SO_3$ is required to increase the T_i of **3e** which contains a methyl end group to the value of **3d** which contains a hydroxy group [Table 2, Fig. 3(*d*, *e*)]. Therefore, qualitatively the ionic interaction generated by 0.85 mol equiv. of $LiCF_3SO_3$ is equivalent to the contribution of one H-bond. The difference between T_i of **6c** and **3d** is 50 °C [Table 1, Fig. 3(*a*)]. This value can be compensated by a complex of **3d** containing about 0.65 mol equiv. of $LiCF_3SO_3$ [Fig. 3(*d*, *e*)]. Therefore, this speculative comparison shows that the methacrylate 'molecular' backbone effect represents the equivalent of a 'supramolecular' backbone generated *via* the interaction of one OH group and 0.65 mol equiv. of $LiCF_3SO_3$ per mol equiv. of **3d**.

An idealized schematic representation of the self-assembled supramolecules formed by these compounds is presented in Fig. 9. Fig. 9(*a*) a shows a representation of the supramolecular assembly formed by the polymer **6d** based on the experimental evidence accumulated so far. Fig. 9(*b*) displays the top view of this supramolecular assembly. The model is drawn to proportion with the experimental values. X-Ray analysis of **6d** at 25 °C provides a column diameter of 60 Å (Table 3). GPC analysis based on polystyrene calibration standards gives a relative average degree of polymerization of 59 (calculated from the M_n in Table 1). The layer thickness is 3.74 Å based on a literature value.[17] Density measurements support an average of about 6 repeat units per layer. Assuming that only one backbone generates this supramolecular segment this results in an approximate column height of 37 Å. The inner core cylinder contains the flexible OE segments and one polymer backbone. Its diameter is approximated at 28 Å which is an unsubstantiated estimate based on molecular modeling. The above picture is idealized since it does not account for defects such as polydispersity, tacticity, or the possibility of more than one polymer chain cooperatively assembling into the centre of the self-assembled cylindrical supramolecule. Additional experiments are required to confirm or invalidate this model.

Fig. 10 presents a representation of the methacrylate and alcohol monomers [Fig. 10(*a*)] being polymerized or self-assembled to form the cylindrically shaped supramolecule as viewed from the top [Fig. 10(*b*)]. X-Ray scattering patterns of the isotropic phase of all **3** and **6** compounds are characterized by a diffuse scattering ring in the low angle region, in addition to the wide angle halo in the 4–5 Å region. This is indicative of the presence of short-range columnar order in the isotropic phase. Residual short-range columnar order is also a characteristic feature of isotropic and nematic phases of discotic molecules. The decrease of cylindrical symmetry of the tubular shaped supramolecule in the isotropic phase is shown in Fig. 10(*b–c*).

Acknowledgements

Financial support by the National Science Foundation (DMR-92-06781), and a NATO travelling grant are gratefully acknowledged. We also thank Professor S. Z. D. Cheng of

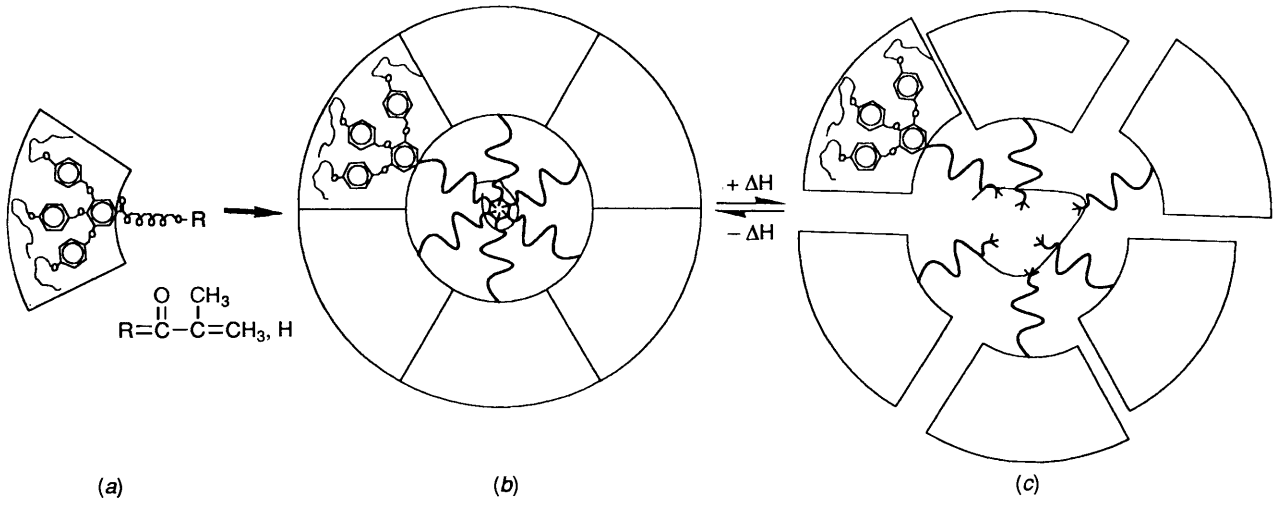

Fig. 10 A top view of the schematic representation of the monomer **5c**: (*a*) being polymerized to the self-assembled cylindrically shaped polymer **6c** in the Φ_h phase; and (*b*) the subsequent partial loss of symmetry of the cylinder when heated above the isotropization temperature

the Department of Polymer Science of the University of Akron for the density measurements.

References

1 (*a*) J. M. Lehn, *Angew. Chem., Int. Ed. Engl.*, 1988, **27**, 89; 1990, **29**, 1304; (*b*) F. Stoddart, *Chem. Brit.*, 1991, 714; (*c*) D. Philp, F. Stoddart, *Synlett*, 1991, 445; (*d*) G. M. Whitesides, J. P. Mathias and C. T. Seto, *Science*, 1991, **254**, 1312; (*e*) J. S. Lindsey, *New J. Chem.*, 1991, 153; (*f*) A. Klug, *Angew. Chem., Int. Ed. Engl.*, 1983, **22**, 565.

2 (*a*) V. Percec, M. Lee, J. Heck, H. Blackwell, G. Ungar and A. Alvarez-Castillo, *J. Mater. Chem.*, 1992, **2**, 93; (*b*) V. Percec, J. Heck, M. Lee, G. Ungar and A. Alvarez-Castillo, *J. Mater. Chem.*, 1992, **2**, 33.

3 V. Percec, G. Johansson, J. Heck, G. Ungar and S. V. Batty, *J. Chem. Soc., Faraday Trans. 1*, 1993, 1411.

4 T. Gramstad and R. N. Haszeldine, *J. Chem. Soc.*, 1956, 173.

5 J. Malthête, N. H. Tinh and A. M. Levelut, *J. Chem. Soc., Chem. Commun.*, 1986, 1548.

6 V. Percec and J. Heck, *J. Polym. Sci. Part A: Polym. Chem.*, 1991, **29**, 591.

7 (*a*) J. M. Lehn, J. Malthête and A. M. Levelut, *J. Chem. Soc., Chem. Commun.*, 1975, 1794; (*b*) J. Malthête, A. M. Levelut and J. M. Lehn, *J. Chem. Soc., Chem. Commun.*, 1992, 1434.

8 D. Tatarsky, K. Banerjee and W. T. Ford, *Chem. Mater.*, 1990, **2**, 138.

9 (*a*) C. Mertesdorf and H. Ringsdorf, *Liq. Cryst.*, 1989, **5**, 1757; (*b*) C. Mertesdorf, H. Ringsdorf and J. Stumpe, *Liq. Cryst.*, 1991, **9**, 337; (*c*) A. Liebmann, C. Mertesdorf, T. Plesnivy, H. Ringsdorf and J. H. Wendorff, *Angew. Chem., Int. Ed. Engl.*, 1991, **30**, 1375.

10 (*a*) G. Lattermann, *Liq. Cryst.*, 1989, **6**, 619; (*b*) G. Lattermann, *Mol. Cryst. Liq. Cryst.*, 1990, **182b**, 299; (*c*) G. Lattermann, S. Schmidt and B. Gallot, *J. Chem. Soc., Chem. Commun.*, 1992, 4091; (*d*) *G. Lattermann, S. Schmidt, R. Kleppinger and J. H. Wendorff, Adv. Mater.*, 1992, **4**, 30.

11 (*a*) S. H. J. Idziak, N. C. Maliszewskyj, P. A. Heiney, P. C. McCauley Jr., P. A. Sprengeler and A. B. Smith III, *J. Am. Chem. Soc.*, 1991, **113**, 7666; (*b*) S. H. Idziak, N. C. Maliszewskyj, G. B. M. Vaughan, P. A. Heiney, C. Mertesdorf, H. Ringsdorf, J. P. McCauley and A. B. Smith III, *J. Chem. Soc., Chem. Commun.*, 1992, 98.

12 (*a*) J. Malthête, A. Collet and A. M. Levelut, *Liq. Cryst.*, 1989, **5**, 123; (*b*) J. Malthête and A. M. Levelut, *Adv. Mater.*, 1991, **3**, 94.

13 (*a*) G. Lattermann, G. Staufer, *Liq. Cryst.*, 1989, **4**, 347; (*b*) G. Lattermann, G. Staufer and G. Brezesinki, *Liq. Cryst.*, 1991, **10**, 169; (*c*) M. Ebert, R. Kleppinger, M. Soliman, M. Wolf, J. H. Wendorff, G. Lattermann, G. Staufer, *Liq. Cryst.*, 1990, **7**, 553; (*d*) R. Festag, R. Kleppinger, M. Soliman, J. H. Wendorff, G. Lattermann and G. Staufer, *Liq. Cryst.*, 1992, **11**, 699.

14 V. Percec, J. Heck, D. Tomazos and G. Ungar, unpublished results.

15 (*a*) J. Collomb, P. Arlaud, A. Gandini, H. Cheradame, in *Cationic Polymerization and Related Processes*, ed. E. J. Goethals ed., Academic Press, New York, 1984, p. 49 and references cited therein; (*b*) Y. Eckstein and P. Dreyfuss, *J. Inorg. Nucl. Chem.*, 1981, **43**, 23; (*c*) A. Loupy and B. Tchouber, *Salt Effects in Organic and Organometallic Chemistry*, VCH, Weinheim, 1992, p. 2.

16 (*a*) P. S. Pershan, *Structure of Liquid Crystal Phases*, World Scientific, Singapore, 1988; (*b*) W. Helfrich, *J. Phys. Colloq.*, C3, 1979, **40**, 3; (*c*) V. Percec, J. Heck and G. Ungar, *Macromolecules*, 1991, **24**, 4957.

17 C. R. Safinya, K. S. Liang, W. A. Varady, N. A. Clark and G. Anderson, *Phys. Rev. Lett.*, 1984, **53**, 1172.

18 *Physics of Amphiphiles: Micelles, Vesicles and Microemulsions*, eds. V. Degiorgi and M. Corti, North Holland, Amsterdam, 1985.

19 (*a*) V. Percec and D. Tomazos, *Molecular Engineering of Liquid Crystalline Polymers* in *Comprehensive Polymer Science*, First Suppl., ed. G. Allen ed., Pergamon Press, Oxford, 1992, p. 299; (*b*) V. Percec, D. Tomazos, *Adv. Mater.*, 1992, **4**, 548.

20 V. Percec, C. G. Cho and C. Pugh, *J. Mater. Chem.*, 1991, **1**, 217, and references cited therein.

Paper 3/02825I
Received 18*th May* 1993
Accepted 5*th August* 1993